Review Articles

IJES *Iranian Journal of Earth Sciences*
Vol. 15, No. 2, 2023, 140-153.
DOI: 10.30495/ijes.2022.1942984.1698

Relationship between Rare Earth and Radioactive Elements

Seyyed Saeed Ghannadpour*[1], Ardeshir Hezarkhani [1]

1. Department of Mining Engineering, Amirkabir University of Technology (Tehran Polytechnic), Tehran, Iran.

Received 6 February 2022; accepted 18 May 2022

Abstract

Based on the relation of radioactive and rare earth elements (REEs) in some of prospecting projects (particularly uranium prospecting) in central Iran, in current study, sampling from the Baghak anomaly in Sangan iron ore mine has been done according to radioactivity for the first time. The purpose of this research is to survey such a relation in a different case study (skarn mine) with central Iran. Optical microscopic and scanning electronic microscopic (SEM) studies along with geochemical and statistical analyses (based on the spider diagrams) are employed. The significant amount of uranium, cerium, lanthanum and high a concentration of REEs in results, along with high amount of iron, is one of the reasons why Baghak anomaly is considered very important. Results show the accumulation of cerium in the allanite lattice (as the solid solution).

Keywords: *Radiation measurement methods, REEs, radioactive elements, Baghak anomaly, Sangan, Iran.*

1. Introduction

The REEs include a set of seventeen elements (the fifteen lanthanides, Sc and Y) (Menendez et al. 2017). The main properties of REEs render them important in polishing compounds, permanent magnets, lighting phosphors and ceramics (Yamin et al. 2017), and also in other technologies, such as atomic energy, aerospace industries, advanced medical, high-powered lasers, and other sensitive technologies (Ghannadpour and Hezarkhani 2022). There are two groups of REEs: light REEs (LREE, e.g. lanthanum, cerium, praseodymium, neodymium, promethium, samarium, and europium) and heavy REEs (HREE, e.g. gadolinium, terbium, dysprosium, holmium, erbium, thulium, ytterbium, lutetium, yttrium, and scandium) (Yang et al. 2017).

Ore minerals hosted REEs are almost formed in all rock types (Hou et al. 2015). The most authoritative classifications for ore deposits of REEs have been proposed by Walters et al. (2010). However, a united global classification for the REEs have been presented from the aspect of mineralization by Orris and Grauch (2002) which is a comprehensive classification (Orris and Grauch 2010). The skarn reserves are epigenetic and metasomatic reserves that are formed in rocks which enriched in carbonates and placed in contact halos of intrusive bodies. From skarn reserves associated with carbonatites which are basically main source of REEs in the world, 200,000 tons of REE oxide (particularly light REEs) has been extracted from a skarn deposit (U-REE-Th), the Mary Kathleen, located in Australia. The mentioned reserve contains 9.5 million tons of ores with a grade of 0.13% U_3O_8. This skarn deposit is hosted by garnet-bearing calcsilicate rocks adjacent to an alkali-granite intrusive body. Uraninite is the main ore mineral and REEs are placed in uraninite, apatite and alunite (Hawkins 1975; Derrick 1977). Numerous studies show that there are REEs in Sangan as an important skarn iron skarn deposit in Khorasan Razavi province, Iran.The concentration of REEs in garnets from the Sangan iron mine was measured by LA-ICP-MS (Boomeri 1998; 2006). Senjedak-I and Ferezneh anomalies (as eastern anomalies) were reported (Mazhari et al. 2015; 2016; 2017). There is a change in the LREE/HREE ratio from 58 to 78 in Ferezneh anomaly. Additionally, an enrichment of light REEs (moderate) and a Eu positive anomaly were observed (Mazhari et al. 2015). In Senjedak-I, REEs show a negative anomaly of Eu, an enrichment of light REEs (moderate), positive pattern of heavy REEs (close to flat), and negative barium, strontium, lanthanum, cerium, titanium and europium anomalies (Mazhari et al. 2016). The enrichment of high field strength elements, zirconium, neodymium, gadolinium, tantalum, yttrium, and hafnium and the barium and strontium depletion were related to a post orogenic granitoids in some eastern anomalies (Golmohammadi et al. 2014). A relative enrichment of light REEs proportion to heavy REEs and enrichment of large ion lithophile element (LILE) proportion to high field strength elements (HFSE), show the magma formation in a subduction zone in several central and western anomalies (Golmohammadi et al. 2013; 2015; Malekzadeh Shafaroudi et al. 2013).The Sangan deposit geochemistry has been studied by Sepidar et al with the aim of determining the conceptual model of hydrothermal fluid evolution (Sepidar et al. 2017). Geochemistry, fluid inclusion characteristics, mineralogy and petrochronology have been also studied by Mehrabi et al. (2021) in a central anomaly (Dardvay). The relationship between these two categories (radioactive and rare earth elements) has been investigated in other studies in Iran (Saghand, located in central Iran (Deymar et al. 2019) and elsewhere in the world (e.g. Vural 2020;

---

*Corresponding author.
E-mail address (es): s.ghannadpour@aut.ac.ir

Cunha et al. 2018; Ling et al. 2006 and etc). It should be also noted that often in uranium prospecting positions, especially, central Iran zone, the REEs enrichment and association are considered as a typical feature (Ghannadpour 2014). In this study, this relation has been investigated more detailed in the case of a Fe-skarn mineralization in the Baghak anomaly. This anomaly is located in Sangan iron mines and are considered as a different mineralization with central Iran mineralizations. The radiation measurement was applied for the first time in this study to achieve an optimized sampling with a low cost for prospecting REEs and sampling is done according to radiation measurement of samples using a spectrometry.

2. Study Area

The Sangan mines complex is located in Khorasan Razavi province (it is 18 kilometres far from south-east of Sangan, 40 kilometres from south-east of Khaf, 68 kilometres from south-west of Tibad and 300 kilometres from south-east of Mashhad (Karimpour and Malekzadeh Shafaroudi 2007; Golmohammadi et al. 2014). The area with 10 kilometres wide and 22 kilometres long includes 3 anomalous parts: a) western, b) central and c) eastern deposits (Fig 1) (Golmohammadi et al. 2015).

The Baghak mine as case study of this research, is located in the Sangan central part. The mentioned anomaly is 200 meters south of Dardvey deposit and in eastern border of northern C (Cn) anomaly. The Baghak deposit covers an area of approximately 260 ha. The latitude and longitude of this anomaly is respectively from 3817100 to 3818600 N and 266500 to 268400 E. There are 239 boreholes with a total length of approximately 63 kilometres. 6641 borehole samples analyses have been carried out (Iran Eastern Iron Ore Co 2011, Jafari and Yazdi 2014; Ghannadpour et al. 2018).The geological map of the Sangan iron ore complex along with western and central anomalies are illustrated in Fig 2 (Golmohammadi et al. 2015).

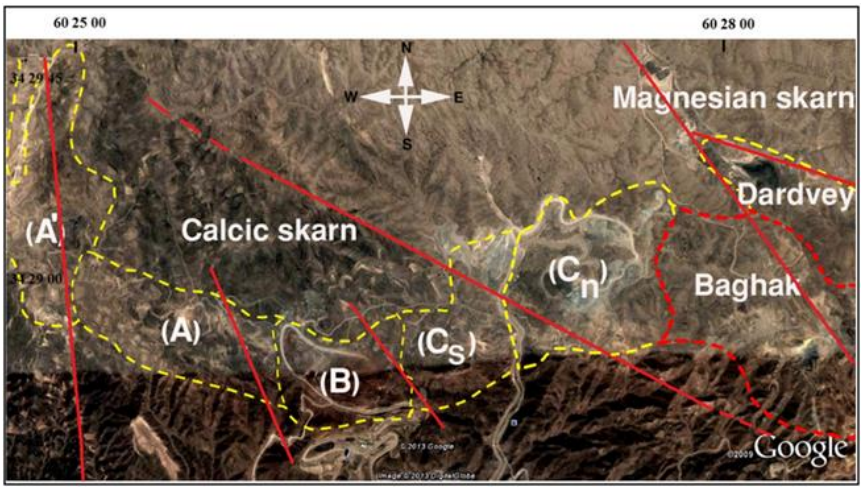

Fig 1. Position of anomalies in the Sangan deposit along with major faults (A', A, B, Cs, and C_N: western anomalies and Dardvey and Baghak: central anomalies).

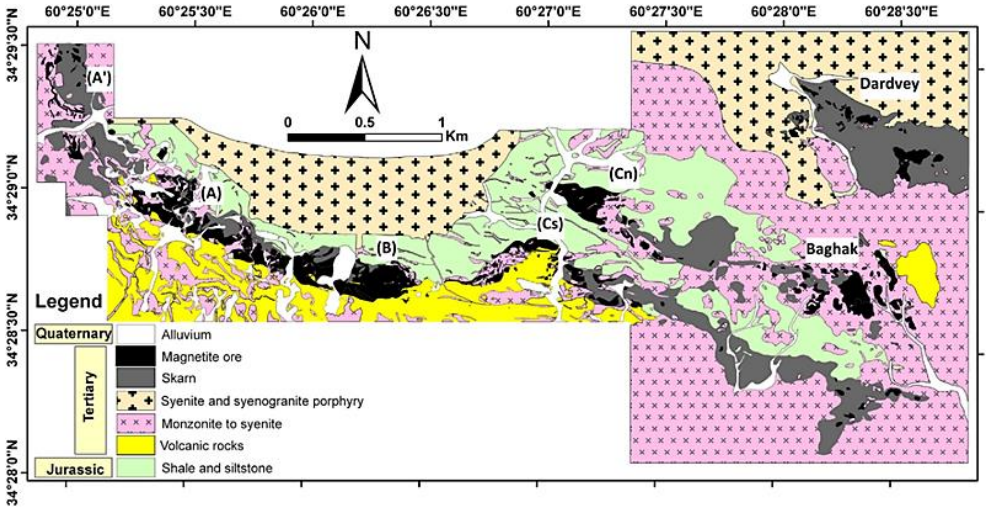

Fig 2. Geological map of Sangan mine and position of western and central anomalies.

3. Sampling and Methodology

Sampling operation has been carried out from drilling cores in view of the relation between radioactive and rare earth elements. Sampling is divided into two parts:

a) Employing logs of some boreholes (if exist, because there are only 24 boreholes in which logging operations, have been carried out).

b) Spectrometry of drilled cores (by a portable hand-held spectrometer) and collecting hot samples in term of radioactivity.

The results of the first part of the sampling could be seen in Fig 3. The maximum amount of radioactivity (CPS: Count per Second) for each borehole is shown on its collar. Accordingly, two priorities are considered for spectrometry operations. Then, after the initial investigation of the drilled cores, the radioactivity information of the area background, the core library and the optimal amount of radioactivity are determined (Table 1).

Table 1. Amount of radioactivity in Baghak mine (CPS).

Area background	200
Core library	250
Optimal threshold	800

Finally, based on the obtained information from Table 1, spectrometry operations are performed on the drilled cores. Accordingly, 151 samples were collected in different lengths from 10 to 300 centimetres.

3.1. Preliminary Investigation

In this section, the data resulted from spectrometry operation (radiometry) are investigated before describing preparation and detailed study of the samples taken in previous section. First, the boreholes which show suitable radioactivity or include significant value of P according to their analyses are determined which are displayed in Figure 4.

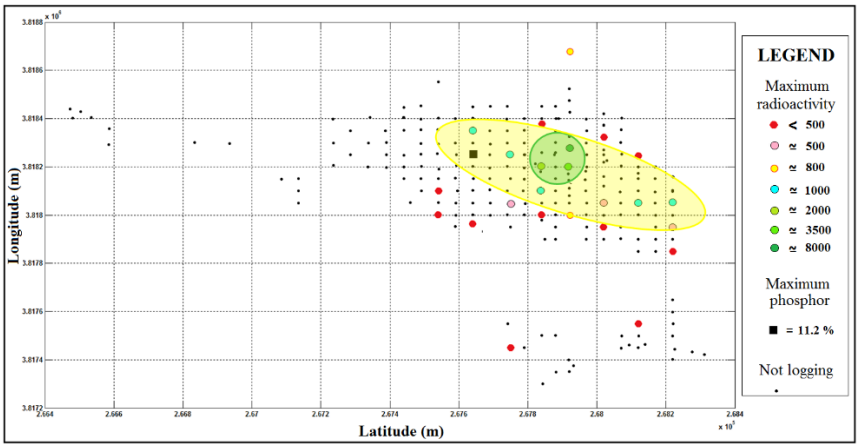

Fig 3. Map showing maximum radioactivity of boreholes on their collars along with dense areas of radioactivity (Green areas: high radioactivity, and yellow areas: optimum radioactivity).

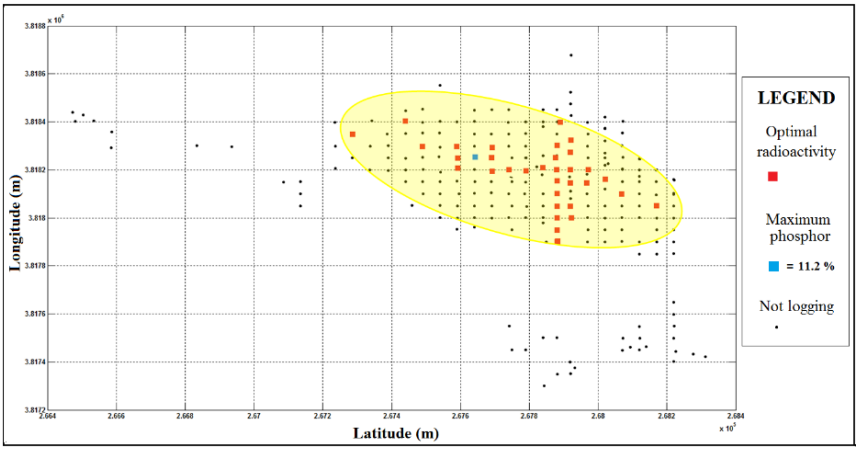

Fig 4. Map showing boreholes and areas which include the optimal radioactivity based on spectrometry results (Yellow areas: optimum radioactivity).

According to this figure, specified region for radioactive samples (radioactive boreholes) is similar to region which was approximately determined before sampling operation using logs from 24 boreholes (Fig 3). In the next step, in order to investigate the relation between radioactive and rare earth elements, the samples containing the most radioactivity are chosen for microscopic studies. The selection of the sections type (thin or polish) for microscopic studies (using optical microscope (Leitz German make) and electronic microscope (SEM XL30, Philips, Netherlands)) are carried out based on the samples radioactivity and macroscopically studies (petrology) that have been reported in Table 2.

Table 2. Samples radioactivity and petrology for preparation of thin or polished sections (CPS is reported based on scintillometer (SPP2 manufactured by SAPHYMO, France); Magnetite: Mag, Pyrite: Py, Amphibole: Amp, Carbonate: Cb, Calcite: Cal, Pyroxene: Px, Phlogopite: Phl, Biotite: Bt, Feldspar: Fsp, Pyrrhotite: Po, Silica: Si and Chloride: Cl).

Sample ID	Petrology	CPS	Section type	Sample ID	Petrology	CPS	Section type
01	Mag-Py-Amp?	350	Thin and Polish	16	Py-Mag-Cal	300	Thin and Polish
02	Py-Amp?	100	Thin and Polish	17	Mag-Py	320	Thin
03	Mag-Py	80-100	Thin and Polish	18	Amp-Cl-Mag	150	Thin and Polish
04	Cb	100	Thin and Polish	19	Mag-Py	300	Thin and Polish
05	Mag-Amp?	250	Polish	20	Mag-Py-Amp?	1000	Thin and Polish
06	Cal-Py-Amp-Px-Mag	300	Thin and Polish	21	Mag-Py-Amp?	400	Thin and Polish
07	Phl-Bt-Py-Fsp	250-300	Thin and Polish	22	Mag-Amp minerals?	300	Thin
08	Po?-Amp?	250-300	Thin and Polish	23	Cb-Si-Phl	200	Thin and Polish
09	Mag-Py-Fsp-Amp?	250-300	Thin and Polish	24	Phl-Bt-Cb-Py	200	Thin and Polish
10	Py -Si -Bt	300	Thin and Polish	25	Cb-Amp	250-300	Thin and Polish
11	Py-Amp-Px	300	Thin and Polish	26	Py-Cb-Amp minerals	300	Polish
12	Py-Mag-Cb	200-230	Polish	27	Py-Cb-Si	250-300	Thin
13	Mag	220	Thin	28	Phl-Bt-Amp-Py	250-300	Thin
14	Cb-Cl-Amp	200	Thin and Polish	29	Phl-Bt-Cb	250-300	Thin
15	Mag-Py-Amp-Px	150	Thin and Polish	30	Phl-Mag-Amp	250	Thin

3.2. Optical microscope studies

In the previous section, from samples with high radioactivity, 27 thin and 24 polished sections are provided that their type is reported in Table 2. Results relative to two sections (thin section: 94-EXP-SN-43-20 and polished section: 94-EXP-SN-30-12) are presented in this section of the article. Four microscopic images from thin section of 94-EXP-SN-43-20 are shown in the Fig 5. Microscopic images of polished section of 94-EXP-SN-30-12 are also illustrated in the Figure 6.

In most sections, significant amounts of allanite and sphene minerals were observed (Fig 7). Moreover, no evidence were observed for the presence of radioactive elements bearing minerals and minerals such as apatite, monazite, xenotime or bastnasite that include REEs (e.g. Figs. 5-6). Given that the amount of allanite and sphene in sections is very high. It is possible that they contain rare earth elements. diamond shaped minerals are observed in this section (Fig 7a). According to apparent features of these minerals, the presence of monazite in this section is probable. However, due to the similarity of this mineral and sphene (Gribble 1988) which are observed abundantly in all sections, SEM studies seem more necessary.

Identifying mentioned minerals become easier and the existing doubt could be removed by one scan and simple investigation in SEM studies, and measuring P, Ca, Ti and Si values. Phosphorus is involved in monazite ((REE) PO_4), but sphene ($CaTiSiO_5$) include no P and in addition, Ca, Ti and Si are involved in that (Gregory et al. 2007). Finally, the study of sections by SEM was on the agenda. Therefore, samples were sent to Amirkabir University of Technology (AUT) SEM laboratory.

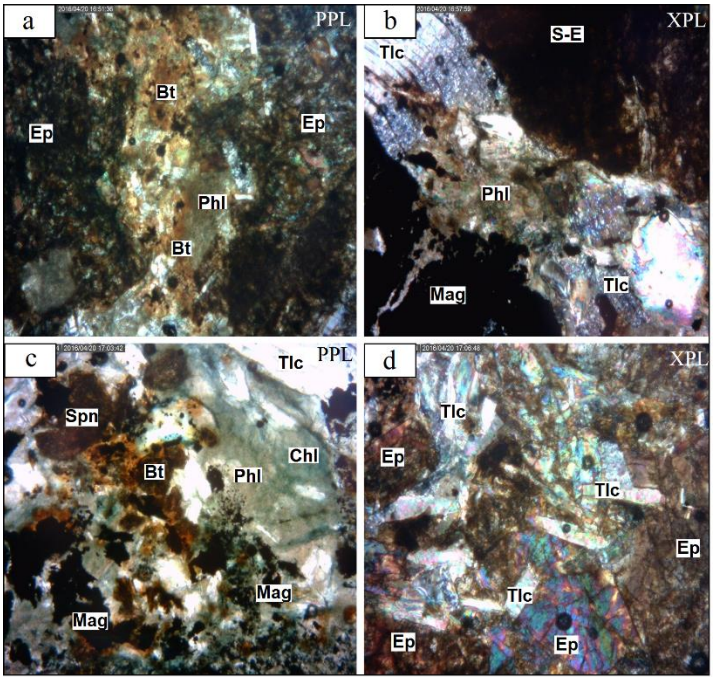

Fig 5. Images of thin section 94-EXP-SN-43-20 (XPL: crossed polarized light and PPL: plane polarized light). a. a set of epidotes is seen on both sides. Biotite is formed in the middle on carbonate and phlogopite with fine texture is seen along with it (original magnification x50), b. A set of sphene-epidote and coarse talc is likely resulted from silicatization of carbonate and also phlogopite overlapped on them and magnetite are seen (original magnification x50), c. Phlogopite-carbonate which has been chlorinated in some parts and scattered talc minerals are seen in it and finally their accompaniment by small minerals such as sphene and magnetite (original magnification x50), d. The accumulation of epidote minerals are associated with dispersed talc minerals. A fine-grained phlogopite is seen in overlapping on the carbonate (original magnification x50). (Bt = biotite, Chl = chlorite, Ep = epidote, Mag = magnetite, Phl = Phlogopite, Spn = sphene, S-E = sphene-Epidote, Tlc = talc, abbreviation of mineral name from study of Whitney and Evans (2010).

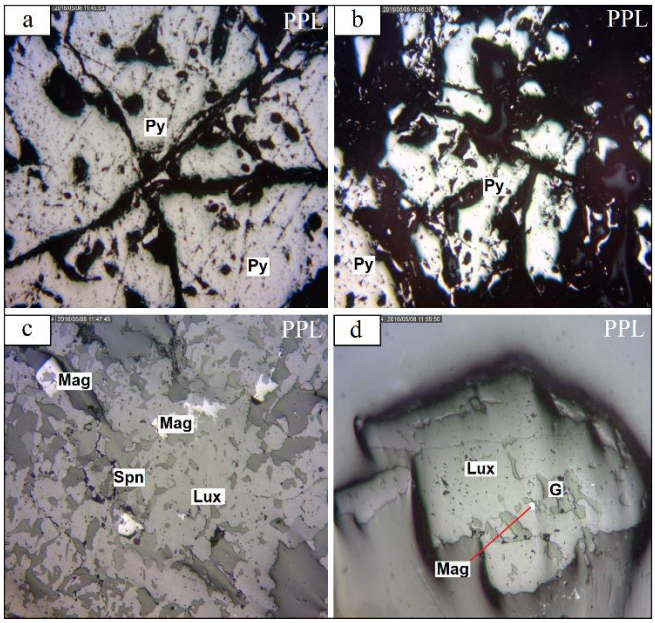

Fig 6. Images of polished section 94-EXP-SN-30-12 (XPL: crossed polarized light and PPL: plane polarized light). a. Pyrite as a large mass of minerals and coarse and fine-grained textures on its surface are seen. Corrosion in the site of the cracks and their intersections are relatively severe (original magnification x100), b. Severe corrosion and fine grained corrosion texture is seen in pyrite (original magnification x100), c. Leucoxene areas along with leakage of gangue to inside it which the small magnetite minerals are dispersed in them. The leakage of gangue to inside of magnetite is seen (original magnification x100), d. Succession leucoxene is seen instead of titanium-magnetite and also small magnetite minerals are seen as the remaining texture. There are gangue leakages into leucoxene (original magnification x50). (G = gangue, Lux = leucoxene, Mag = magnetite, Py = pyrite, Spn = sphene, abbreviation of mineral name from study of Whitney and Evans (2010).

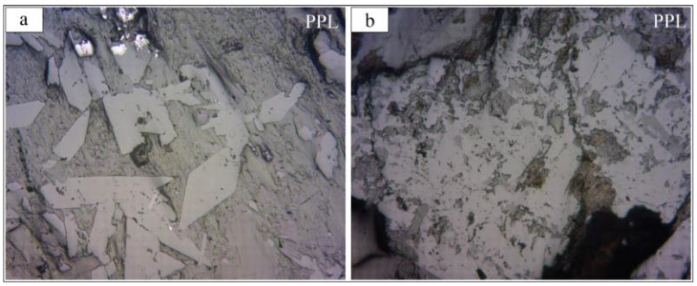

Fig 7. Zones contain allanite and sphene in polished sections (original magnification x50; XPL: crossed polarized light and PPL: plane polarized light). a. sphene which are similar to monazite (94-EXP-SN-34-16), and b. allanite and sphene minerals (polished section 94-EXP-SN-30-12).

3.3. Results of SEM Study

After scanning uranium (Fig 8b), it was determined that the light spot in figures (Figs. 8a, 9a, b) are corresponded to U-bearing mineral. According to Figs. 9c, it is observed that the lighter mineral (Figs. 9a, b) is corresponded to Fe (magnetite) and surrounding minerals (dark and light grey coloured minerals) based on significant amount of Si (Fig 9d) and Ca (Fig 9e) corresponds to epidote. It could be noted that Ce is located in the network of epidote (allanite) in this study (Fig 9f).

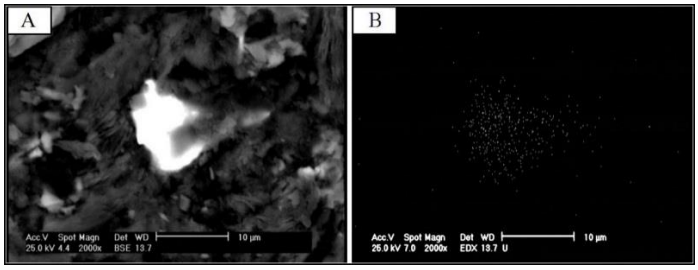

Fig 8. a. Uranium in thin section with sample ID 94-EXP-SN-43-20, b. scanning for uranium at the scale of 10 micrometers from part A.

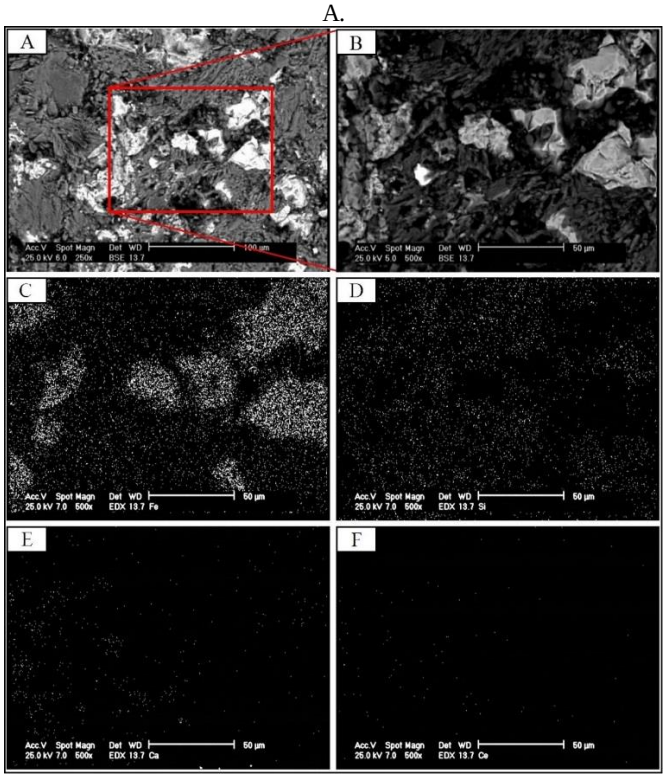

Fig 9. a. Displaying allanite, iron and uranium in thin section with sample ID 94-EXP-SN-43-20, b. Magnification from part A, c. Scan result for Fe, d. Scan result for Si, e. Scan result for Ca, f. Scan result for Ce.

Therefore, surrounding minerals (dark and light grey coloured minerals) in Fig 9a are considered as allanite. As it is observed, U is displayed in the REEs-bearing minerals (allanite). According to Figs. 8 and 9, uranium is lighter than other elements because its specific weight is more than other elements, such as iron or REEs. In Figs. 9a, b, Fe is displayed lighter than the other elements and minerals duo to the same reason mentioned above.In this section, by studying and investigating first thin section, probability of the presence of REEs in allanite is highlighted. Thus, studying other sections will be efficient in the certain happing of this probability. After SEM studies on polished section of 94-EXP-SN-43-20, several photos are provided from another polished section (94-EXP-SN-30-12) (Fig 10) which are going to be discussed in the following. After scanning uranium (Fig 10d), it was determined that the light spot in this figure (Figs. 10a, b, c) are corresponded to U-bearing mineral. The scanning process was again performed for two Fe and S elements (Figs. 10e, f). As seen in this figure, minerals that are located next to uranium (Figs. 10a, b, c) are likely to be pyrite or pyrrhotite, due to the presence of iron and sulfur. The probability of pyrite is more than that of pyrrhotite due to the low amount of sulfur scanned by the microscope. Therefore, as it is observed, U is displayed in the Fe-bearing minerals. Study results of section 94-EXP-SN-34-16 show the presence of La and Nd based on scans that carried out on the dark and light grey coloured minerals. Moreover, diamond shaped minerals which are observed in this section and caused the doubt of the presence of monazite, are investigated that SEM resulted photo along with a brief description is presented in the following.

No evidence for the presence of monazite were observed in REE scanning results from shaped minerals that they were assumed to be probably monazite before (Fig 7a). In other words, the result of P-scanning in shaped minerals was negative. Therefore, according to microscopic studies, it was confirmed that shaped minerals correspond to sphene. Light spots are determined to be Fe-bearing minerals according to the Fe-scanning. Finally, it can be said that REEs, especially Ce are present in the samples (La and Neodymium (Nd) are also observed at a section) and they have been aggregated as solid solution in allanite minerals. Moreover, it is seen that uranium has been mostly trapped as inclusions in empty spaces of allanite (Fig 9) and also Fe-bearing minerals (Fig 10).

3.4. Geochemical analysis of Samples

In order to geochemically analyse the samples, they were sent to ZarAzma laboratory that located in Tehran, Iran.

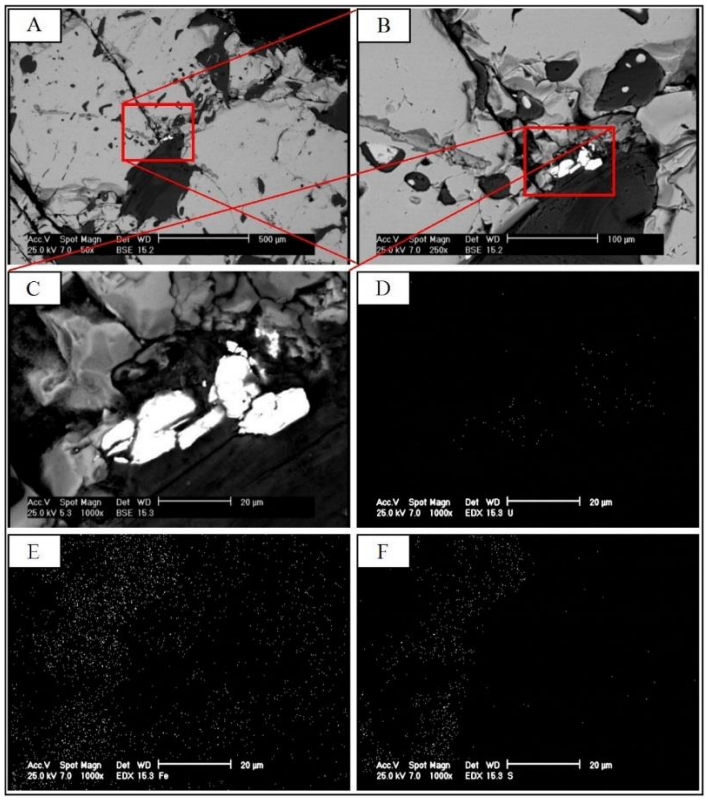

Fig 10. a. Displaying iron and uranium in polished section with sample ID 94-EXP-SN-30-12, b. Magnification from part A, c. Magnification from part B, d. U scan result, e. Fe scan result, f. S scan result.

It should be noted that in addition to 151 abovementioned samples, 2 SRMs (Secondary Reference Materials) were selected for checking the accuracy and 10 duplicate samples for checking the precision. The whole procedure of sample preparation had been done in the AUT laboratory before they were sent to ZarAzma (in order to analyse for major and trace elemental concentration by the ICP-MS). The 56-element analysis results along with the detection limit of the measuring device are reported in Table 3. For analysing the results, investigating the relation between radioactive and rare earth elements, geochemical data are processed in this section. At the first, statistical preprocessing are applied on the data and then, univariate statistical investigations are employed. Finally, multivariate statistical analysis are used.

Table 3. Detection limits of elements measured by ICP-MS (ppm).

	Ag	Al	As	Ba	Be	Bi	Ca	Cd	Ce	Co	Cr	Cs
Detection limit×10^{-2}	10	10000	10	100	20	10	10000	10	50	100	100	50
	Cu	Dy	Er	Eu	Fe	Gd	Hf	In	K	La	Li	Lu
Detection limit×10^{-2}	100	2	5	10	10000	5	50	50	10000	100	100	10
	Mg	Mn	Mo	Na	Nb	Nd	Ni	P	Pb	Pr	Rb	S
Detection limit×10^{-2}	10000	500	10	10000	100	50	100	1000	100	5	100	5000
	Sb	Sc	Se	Sm	Sn	Sr	Ta	Tb	Te	Th	Ti	Tl
Detection limit×10^{-2}	50	50	50	2	10	100	10	10	10	10	1000	10
	Tm	U	V	W	Y	Yb	Zn	Zr				
Detection limit×10^{-2}	10	10	100	100	50	5	100	500				

3.4.1. Geochemical data processing (Univariate analysis)

For statistical processing of investigating elements in Baghak study area (151 samples), first the incorrect data (any typos, outliers or additional characters) are revised in data bank. Then censored data are removed or replaced by substitute values.

Accordingly, scandium and iron have been removed (because the number of censored data is more than the allowed limit (>15%)). But, in the case of other elements, the censored data replaced by appropriate values.

In the next step, average grade (weighted average) for 151 samples are calculated and presented in Table 4.

Table 4. Average grade of considered elements (ppm).

Element	Average
U	185.62
Th	25.93
K	14454.14
Y	35.34
La	958.76
Ce	1125.86
Pr	99.91
Nd	262.48
Er	4.27
Lu	.44
Eu	4.39
Gd	18.75
Tb	2.16
Dy	8.82
Sm	23.36
Tm	.53
Yb	3.28
∑ REE	2548.37

According to Table 4, radioactivity in the study area is only originated from Uranium and considering high concentration of REEs, their correspondence seems more apparent. Actually, this relation is going to be studied in detail by univariate analyses and computing correlation in the following.

The distribution of all elements are investigated for computing the correlation between their grades in the study area. Then, if the data are not normally distributed, different techniques and transformations are applied for normalizing. Finally, according to considering data distribution, correlation method is selected and calculated.Identical composites should be considered for the length of investigating samples and then, detailed analysis can be carried out. The greatest common divisor of the length of samples is considered as the criterion length and samples are extended to 5 cm length composites. The result is generating 2257 samples by the length of 5 cm.Surveying of data distribution shows that grades related to 19 investigating parameters do not follow normal distribution. Bivariate and trivariate logarithmic transformations, and also inverse, box-cox and Johnson transformations did not work efficiently for normalizing, since final results from calculating W index not only approached zero (Hezarkhani and Ghannadpour 2015; Ghannadpour and Hezarkhani 2016 and 2018), but significant decrease could be observed (Fig 11). Moreover, Kolmogorov-Smirnov test also shows that data distribution do not follow normal distribution after applying mentioned transformations.

Since Spearman correlation coefficient needs less presumptions such as normal distribution of the data, despite more efficiency of Pearson correlation coefficient, it is applied for calculating the correlation.

3.4.1. Multivariate Statistical Analysis

Correlation coefficient between the grade of radioactive and rare earth elements and also radioactivity (CPS) is determined in this section for studying their relation. As mentioned in previous section, Spearman correlation coefficient is employed for investigating correlation about non normal distribution data (Table 5). In the next step, correspondence analysis is used to separate anomalous variables (elements) in Baghak mine. Correspondence analysis is a statistical multivariate method, in which simultaneous relation of variables and samples is investigated in one diagram (Cuadras and Cuadras 2006; Greenacre 2016). Results from this analysis could be presented in two forms. First, one or several scatter plots are used that it is called factor correspondence analysis. Second, a dendrogram is used and it is called cluster correspondence analysis.

Actually, determining anomalous variables using factor correspondence analysis is targeted in this section. A 151 * 17 matrix named G consisting of rare earth and radioactive elements is provided as input to the mentioned method. Results of applying this method are based on selecting three eigenvalues from all calculated eigenvalues which cover more than 99% of total variability. Therefore, the study is based on a tri-factor model which is carried out in three scatter plots (Fig 12).

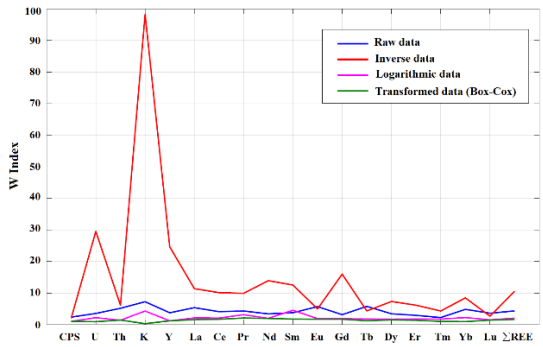

Fig 11. W Indexes for transformed data.

Table 5. Coefficients of Spearman's correlation.

Coefficients of Spearman's correlation															
	Y	La	Ce	Pr	Nd	Sm	Eu	Gd	Tb	Dy	Er	Tm	Yb	Lu	REEs
U	.7	.71	.72	.71	.71	.71	.63	.71	.72	.71	.71	.66	.71	.73	.71
Th	.83	.83	.86	.88	.89	.9	.86	.89	.87	.87	.85	.84	.82	.81	.86
K	.5	.45	.46	.46	.48	.49	.45	.48	.51	.52	.54	.57	.59	.6	.47
CPS	.59	.61	.61	.59	.58	.58	.49	.58	.61	.59	.6	.56	.63	.63	.6

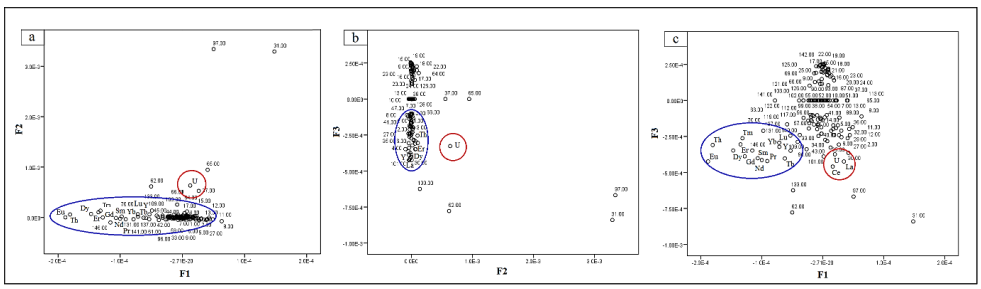

Fig 12. Dispersion diagram of derived factors from correspondence analysis method in Baghak mine. a. The first and second factors, b. The second and third factors, c. The first and third factors.

As it is shown in Figs. 12a and 12b Uranium as anomalous element has been separated well from the others. In Fig 12c, it is observed that by plotting two factors of F1 and F3, Ce and La joined U and separated themselves from other elements and they are placed far from other REEs and radioactive elements. This shows the separation of U, Ce and La as anomalous variables from other studying variables. It should be noted that the precision of this separation could be verified based on reported values in Table 5. Since in mentioned table, it could be seen that reported values for U, Ce and La are much higher than the other investigating values.

3.4.2. Spider Diagrams Analysis

In this section, the average value of 151 samples, are employed for drawing spider diagrams and then, they are analysed. In fact, by doing so, one samples represents total samples belong to all boreholes. Then, spider diagram of chondrite normalized REEs is provided for abovementioned group (Fig 13).

In the above diagram, the europium depletion could be seen compared to with other elements that the plagioclase crystallization (from mineralization magmatism) could be its reason (Malekzadeh Shafaroudi et al. 2013). LREE enrichment compared to the declining trend of HREE could also be observed that is related to the subduction zone magma. (Gill 1981; Rollinson 1993; Wilson 2007; Golmohammadi et al. 2015). Primitive mantle normalized trace and rare earth elements pattern for REEs is shown in Figure 14.

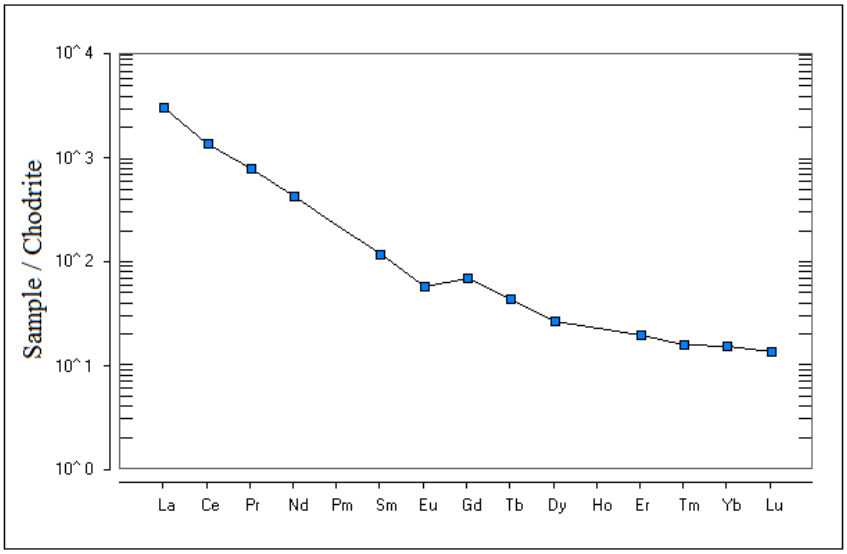

Fig 13. Pattern of chondrite normalized REEs (values from Boynton 1983).

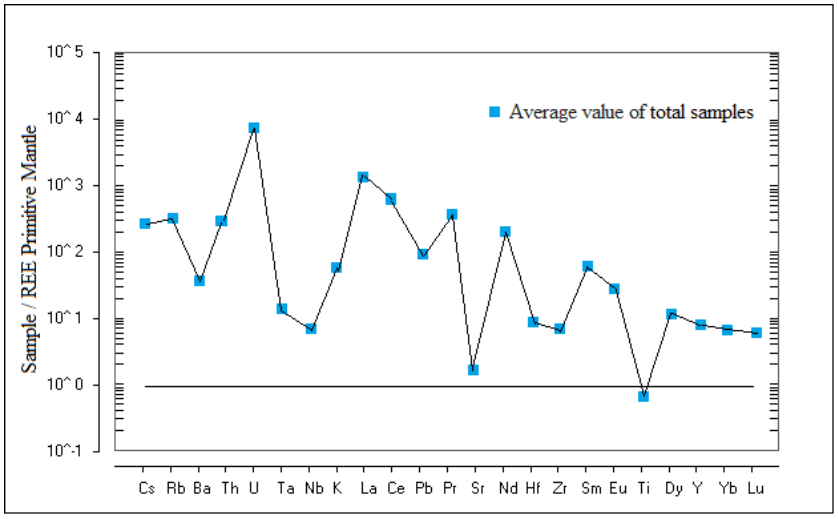

Fig 14. Pattern of primitive mantle normalized rare earth and trace elements (values from McDonough 1995).

In the above diagram, enrichment is clearly evident about cerium, lanthanum, praseodymium, neodymium and uranium.
It is also observed enrichment of LILE such as caesium, rubidium, barium, and potassium and radiative elements (uranium and thorium) and a depletion in HFSE such as niobium, yttrium, titanium, tantalum, and zirconium and HREE (ytterbium and lutetium) (depletion of titanium is compared to the primitive mantle).
The features observed are related to the subduction zone magma in the calcalkaline volcanic arcs of continental active margins (Gill 1981; Pearce 1983; Walker 2001).

4. Discussion

The statistical results imply that the case study involves high amount of uranium, cerium, lanthanum and significant concentration of rare earth elements. This fact is also observed well in results from correspondence analysis that uranium, lanthanum and cerium as anomalous variables (elements) are separated from other investigating variables. Based on the reported elemental analysis, it was specified that:
- Reported correlation coefficients between rare earth elements and radioactivity, uranium and thorium concentration are respectively 0.6, 0.7 and 0.85 which are high and acceptable values.
- The main share in radioactivity in Baghak deposit belongs to uranium, and potassium involves less share of radioactivity.
- Th concentration in analysis results was reported as low as the background value, but statistical investigating of mentioned results shows that Th despite low concentration in Baghak anomaly, is suitably related to the REEs and little enrichment which is shown along with REEs, states the formation of this element with REEs from the aspect of metallogeny and geochemistry.
Therefore, according to statistical analysing, a similar relationship (with central Iran mineralizations) was observed in a skarn mineralization. REEs show also a thermodynamic behaviour similar to uranium and thorium. In fact, they are part of large-ion lithophiles and similar to high-reactive lithophile metals like Th, U, P and K. These kind of elements due to strong ionic bond with oxygen as bivalence and trivalence, are placed in a diverse spectrum of silicate and oxide minerals and scattered in continental crust (Ghannadpour and Hezarkhani 2021). Based on geochemical and mineralogical studies and also observing LREE in allanite lattice using SEM, it could be acknowledged that rare earth elements have accumulated as solid solution in the lattice of silicate minerals (particularly allanite minerals). The structural formula of epidote group is $A_2M_3(SiO_4)(Si_2O_7)(O,F)(OH)$, in which A= U, Th, Sr, Ca, REE^{3+}, Pb^{2+} and Mn^{2+}; and M= Mg, Al, Mn^{2+}, Mn^{3+}, Fe^{2+}, Fe^{3+}, V^{3+} and Cr^{3+} (Deer et al. 1986; Gieré and Sorensen 2004). There are three different M sites (M_1, M_2, and M_3) and two structurally different A sites (A_1 and A_2), (Dollase, 1971; Ueda, 1995; Gieré and Sorensen 2004). In group of this minerals, trivalent REEs are located at the A sites, which in the epidote, the both endmembers contain calcium. The REE^{3+} bond is usually balanced by using a divalent cation (Mg, Mn^{2+} Fe^{2+}) instead of a trivalent cation at the M sites.
Allanites as enriched mineral (in terms of REEs) of the epidote group are common lateral phases in sedimentary, metasomatic, metamorphic and igneous rocks. There are small amounts of REEs in most minerals in the epidote group, while they are essential structural components in allanite and also its associated minerals such as androsite, khristovite, dollaseite, ferriallanite and dissakisite (Gieré and Sorensen 2004). The idealized $CaREEAl_2Fe^{2+}Si_3O_{11}O(OH)$ formula could be employed to represent allanite (Ercit 2002). In fact, allanite is related to epidote by the coupled substitution: $REE^{3+} + Fe^{2+} \leftrightarrow Ca^{2+} + Fe^{3+}$
Allanite along with ferriallanite (Gieré and Sorensen 2004; Kartashov et al. 2002) are the only members of the epidote group that Fe^{2+} is an essential constituent in their composition. In fact, in the epidote group, the most diverse part belongs to allanite. Allanite-(Ce) as The most common type of allanite, has the formula $(Ce,Ca,Y)_2(Al,Fe^{2+},Fe^{3+})_3(SiO_4)_3(OH)$. Although this formula describes allanite-(Ce) well, but it is not the most complete form of its formula. In mineralogical and geochemical studies of Zafarabad in Kurdistan province, Iran (Barati and Gholirpour 2014), it is concluded that the reason for enriching light REEs compared to the heavy REEs (this enrichment is also present in Baghak samples), is light REEs entry into the magnetite lattice. Because magnetite could contain up to 67.6% by weight of calcium. In the mentioned study, it was said that it is possible for REEs ions to enter the magnetite lattice because their ion radius are similar to calcium (replacement instead of Ca) (Barati and Gholirpour 2014). Whereas SEM studies results rule this out about the magnetites of Baghak. This results at the Baghak anomaly show that there are REEs especially the Ce only in the allanite lattice and they are not found in the magnetite lattice and Fe-bearing minerals.
Thus, it is likely that REEs ions have been entered as solid solutions into the allanite lattice and in fact, their light (LREE) have been replaced instead of Ca in the allanite lattice. This is also true for thorium. But due to the poor mineralization fluid (in term of Th), there is no significant enrichment for it. Therefore, this small amount sits next to the REEs in the silicate lattice of allanite. Whereas, uranium is independent of the silicate lattice of allanite.

5. Conclusions

Results obtained from spider diagrams confirm that plagioclase-bearing was the source magma and features observed are related to the subduction zone magma.
The statistical studies results imply anomalous state of U, Ce and La (that have aggregated as solid solution in allanite lattice and even Fe-bearing minerals which has been trapped in empty space of these minerals as

inclusion). Actually, radioactivity in the study area is entirely affected by uranium and REEs show acceptable correlation with radioactivity and consequently uranium. It was also shown that Th despite low concentration has a suitable correlation with REEs due to similar thermodynamic and geochemical behaviour. Therefore, it was concluded from the results that this relation is explicitly observed in another mineralization type, meaning Sangan skarn iron ore deposit. In fact, prospecting REEs in this anomaly could be known related to the sampling pattern presented in this study. Thus, based on the results from this and former studies, introduced sampling pattern (based on methods of measuring radioactivity) is introduced as an efficient pattern for prospecting REEs. The presented prospecting idea and pattern for exploring REEs in this study could provide an appropriate viewpoint in exploration industry of these elements for decision makers.

Acknowledgements

We are grateful to the SIOC for giving us the data.

References

Barati M, Gholirpour M (2014) Mineralogy, geochemistry and origin of Zafarabad iron ore deposit in Kurdistan using rare earth element data of Magnetite mineral *Journal of Economic Geology* 5(2): 235-254 (in Persian).

Boomeri M (1998) Petrography and geochemistry of the Sangan iron skarn deposit and related igneous rocks, northeastern Iran. PhD thesis, Akita University, Japan, 226 p.

Boomeri M (2006) Rare earth elements (REE) in garnet of Sangan iron ore deposit. Geological Society of Iran, Tehran Tarbiat Moallem University, Tehran, Iran (in Persian).

Boynton WV (1983) Cosmochemistry of the rare earth elements: meteorite studies", in: P. Henderson (editor), Rare earth element geochemistry, Elsevier, Amsterdam, *chapter* 3: 63-114.

Cuadras CM, Cuadras D (2006) A parametric approach to correspondence analysis. *Linear Algebra and Its Applications* 417: 64–74.

Cunha CSM, Escobar MEO, da Silva YJAB, do Nascimento CWA (2018) Spatial variability and geochemistry of rare earth elements in soils from the largest uranium–phosphate deposit, *Environmental Geochemistry and Health* 40: 1629–1643.

Deer WA, Howie RA, Zussman J (1986) Rock-forming minerals, vol. 1B: Disilicates and ringsilicates (2nd edition). Longman, Harlow, United Kingdom.

Derrick GM (1977) Metasomatic history and origin of uranium mineralization at Mary Kathleen, northwest Queensland, *BMR Journal of Australian Geology &* Geophysics 2: 123-130.

Deymar S, Behzadi M, Yazdi M (2019) Relation of alkali-metasomatism and Ti-REE-U (Th) mineralization in the Saghand mining district, Central Iran, *Journal of Economic Geology* 10(2): 471-296.

Dollase W A (1971) Refi nement of the crystal structures of epidote, allanite and hancockite, *American Mineralogist* 56: 447-464.

Ercit TS (2002) The mess that is 'allanite'. *The Canadian Mineralogist* 40: 1411-1419.

Ghannadpour SS (2014) Geochemical and metallurgical studies of rare earth elements and evaluating their potential in Bafq-Robat Posht-e Badam belt. Atomic Energy Organization of Iran (Under Supervision of I.R.IRAN National Elites Foundation). Tehran, Report, 162 p (in Persian with English abstract).

Ghannadpour SS, Hezarkhani A (2016) Introducing 3D U-statistic method for separating anomaly from background in exploration geochemical data with associated software development, *Journal of Earth System Science* 2: 387-401.

Ghannadpour SS, Hezarkhani A (2018) Providing the bivariate anomaly map of Cu–Mo and Pb–Zn using combination of statistic methods in Parkam district, Iran, *Carbonates and Evaporites* 33(3): 403-420.

Ghannadpour SS, Hezarkhani A (2021) Investigation of geochemical correlation between radioactive and rare earth elements; case study of Baghak mine, NE of Iran, *Journal of Mining and Environment* 12(2): 569-587.

Ghannadpour SS, Hezarkhani A (2022) Prospecting rare earth elements (REEs) using radiation measurement: case study of Baghak mine, Central Sangan iron ore mine, NE of Iran, *Environmental Earth Sciences* 81: 363. https://doi.org/10.1007/s12665-022-10479-6

Ghannadpour SS, Hezarkhani A, Golmohammadi A (2018) Applying 3D U-statistic method for modeling the iron mineralization in Baghak mine, central section of Sangan iron mines, *Geosystem Engineering* 21(5): 262-272.

Gieré R, Sorensen SS (2004) Allanite and Other REE-Rich Epidote-Group Minerals, *Reviews in Mineralogy & Geochemistry* 56: 431-493.

Gill JB (1981) Orogenic Andesites and Plate Tectonics. Springer-Verlag, Berlin, 390 p.

Golmohammadi A, Karimpour MH, Malekzadeh Shafaroudi A, Mazaheri SA (2013) Petrology and U-Pb zircon dating of intrusive rocks from A, C-south, and Dardvay districts, Sangan iron stone mine, Khaf, *Journal of Economic Geology* 2(5): 157-174 (in Persian with English abstract).

Golmohammadi A, Karimpour MH, Malekzadeh Shafaroudi A, Mazaheri SA (2015) Alteration-mineralization, and radiometric ages of the source pluton at the Sangan iron skarn deposit, northeastern Iran, *Ore Geology Reviews* 65(2): 545-563.

Golmohammadi A, Mazaheri SA, Karimpour MH, Malekzadeh Shafaroudi A (2014) Zircon U-Pb dating and geochemistry of Sarkhar and Bermani granitic rocks, East of Sangan iron mine, Khaf, *Journal of Petrology* 5(17): 83-102 (in Persian with English abstract).

Greenacre M (2016) Correspondence Analysis in Practice. 3th Edition. Chapman & Hall / CRC, Boca Raton, Florida, 310 p.

Gregory CJ, Rubatto D, Allen C, Williams IS, Hermann J (2007) Ireland TR. Allanite micro-geochronology: a SHRIMP and LA-ICP-MS study, *Chemical Geology* 245: 162–182.

Gribble CD (1988) Rutley's Elements of Mineralogy. 27th Edition. Unwin Hyman, London.

Hawkins BW (1975) Mary Kathleen Uranium Deposit; in Knight, C. L. (Editor)-Economic Geology of Australia and Papua New Guinea, volume 1. Metals. *Institute of Mining and Metallurgy Monograph Series* 5: 398-402.

Hezarkhani A, Ghannadpour SS (2015) Exploration Information Analysis, first ed. Amirkabir University of Technology (Tehran Polytechnic) press, Tehran (in Persian).

Hou Z, Liu Y, Tian S, Yang Z, Xie Y (2015) Formation of carbonatite-related giant rare-earth-element deposits by the recycling of marine sediments. *Science Report* 5: 10231.

Iran Eastern Iron Ore Co. (2011) Modelling, type's classification, and calculation of iron deposit in Baghak mine. Report, Sangan Iron Ore Complex.

Jafari HR, Yazdi A (2014) Radioactive Anomalies in 1: 50000 Dehbakri Sheet, South of Kerman Province, Iran, *Open Journal of Geology* 04(08):399-405.

Karimpour MH, Malekzadeh Shafaroudi A (2007) Skarn Geochemistry - Mineralogy and Petrology of Source Rock Sangan Iron Mine, Khorasan Razavi, Iran, Scientific Quaterly Journal, *Geosciences* 17(65): 108-125 (in Persian with English abstract).

Kartashov PM, Ferraris G, Ivaldi G, Sokolova E, McCammon CA (2002) Ferriallanite-(Ce), $CaCeFe(SiO_4)(Si_2O)O(OH)$, a new member of the epidote group: Description, X-Ray and Mössbauer study, *The Canadian Mineralogist* 40:1641-1648.

Ling M, Yang X, Sun W, Miao J, Liu C (2006) REE/trace element characteristics of sandstone-type uranium deposits in the Ordos Basin, *Chinese Journal of Geochemistry* 25(4): 354-364.

Malekzadeh Shafaroudi A, Karimpour MH, Golmohammadi A (2013) Zircon U-Pb geochronology and petrology of intrusive rocks in the C-North and Baghak districts, Sangan iron mine, NE Iran, *Journal of Asian Earth Sciences* 64: 256-271.

Mazhari N, Malekzadeh Shafaroudi A, Ghaderi M (2015) Geology, mineralogy and geochemistry of Ferezneh ferromanganese anomaly, east of Sangan mines complex, NE Iran, *Journal of Economic Geology* 7(1): 23-37.

Mazhari N, Malekzadeh Shafaroudi A, Ghaderi M (2016) Geochemistry of intrusive rocks, petrology of skarn, and mineralogy and chemistry of orebodies in Senjedak-I area, east of Sangan mine, Khaf, NE Iran, Scientific Quaterly Journal, *Geosciences* 25(100): 235-246 (in Persian with English abstract).

Mazhari N, Malekzadeh Shafaroudi A, Ghaderi M (2017) Detecting and mapping different types of iron mineralization in Sangan mining region, NE Iran, using satellite image and airborne geophysical data, *Geoscience Journal* 21: 137-148.

McDonough WF, Sun SS (1995) The composition of the Earth, *Chemical Geology* 120: 223-254.

Mehrabi B, Ghasemi Siani M, Zhang R, Neubauer F, Lentz DR, Tale Fazel E, Karimi Shahraki B (2021) Mineralogy, petrochronology, geochemistry, and fluid inclusion characteristics of the Dardvay skarn iron deposit, Sangan mining district, NE Iran, *Ore Geology* Reviews 134: 104146.

Menendez A, James RH, Roberts S, Peel K, Connelly D (2017) Controls on the distribution of rare earth elements in deep-sea sediments in the North Atlantic Ocean, *Ore Geology Reviews* 87: 100-113.

Orris GJ, Grauch RI (2002) Rare Earth Element Mines, Deposits, and Occurrences. *Open-File Report* 02-189. Reston, VA: USGS.

Pearce JA (1983) Role of the sub-continental lithosphere in magma genesis at active continental margins. in: Hawkesworth, C.J., Norry, M.J. (Eds.), Continental Basalts and Mantle Xenoliths, Shiva, Nantwich, 230–249.

Pearce JA, Parkinson IJ (1993) Trace element models for mantle melting: application to volcanic arc petrogenesis. in: Prichard, H.M., Albaster, T., Harris, N.B.W., Neary, C.R. (Eds.), Magmatic Processes in Plate Tectonics. *Geological Society of London Special Publication* 76: 373–403.

Rollinson H (1993) Using geochemical data, Evaluation, Presentation, Interpretation, Harlow. Longman Scientific & Technical, Harlow, UK, 352 p.

Sepidbar F, Sepidbar H, Li JW, Wei C, George LL, Burlinson K (2017) Mineral geochemistry of the Sangan skarn deposit, NE Iran: Implication for the evolution of hydrothermal fluid, *Chemie der Erde* 77: 399–419.

Ueda T (1995) The crystal structure of allanite, $OH(Ca,Ce)2(FeIIIFeII)Al_2OSi_2O_7SiO$. Memoirs of the College of Science, University of Kyoto, *Series B* 22/2:145-163.

Vural A (2020) Investigation of the relationship between rare earth elements, trace elements, and major oxides in soil geochemistry, *Environmental Monitoring and Assessment* 192 (2): 124.

Walker JA, Patino LC, Carr MJ, Feigenson MD (2001) Slab control over HFSE depletions in central Nicaragua, *Earth and Planetary Science Letters* 192: 533–543.

Walters A, Lusty P, Chetwyn C, Hill A (2010) Rare earth elements. Mineral Profile SeriesBritish Geological Survey, United Kingdom, 45 p.

Whitney D L, Evans B W (2010) Abbreviations for names of rock-forming minerals, *American Mineralogist* 95: 185–187.

Wilson M (2007) Igneous Petrogenesis: A Global Tectonic Approach. Springer (Originally published by Chapman & Hall), Netherlands, 466 p.

Yamin D, Xiangguang G, Yanliang W, Zeyuan Z, Chao H, Xiaoqi S (2017) A separation processing for industrial rare earth feed solution by phosphonium ionic liquid type saponification strategy, *Journal of Rare Earths* 35(3): 290-299.

Yang Z, Ruilian Y, Gongren H, Xiaohui L, Xianrong L (2017) Characteristics and environmental significance of rare earth elements in PM2.5 of Nanchang, China, *Journal of Rare Earths* 35(1): 98-105.